ACS Sustainable Chemistry & Engineering

pubs.acs.org/journal/ascecg

Research Article

Aqueous Processing of $LiCoO_2$–$Li_{6.6}La_3Zr_{1.6}Ta_{0.4}O_{12}$ Composite Cathode for High-Capacity Solid-State Lithium Batteries

Ruijie Ye,* Martin Ihrig, Egbert Figgemeier, Dina Fattakhova-Rohlfing, and Martin Finsterbusch

Cite This: *ACS Sustainable Chem. Eng.* 2023, 11, 5184–5194

Read Online

ACCESS | Metrics & More | Article Recommendations | Supporting Information

ABSTRACT: To fabricate ceramic composite cathodes $LiCoO_2$–$Li_{6.6}La_3Zr_{1.6}Ta_{0.4}O_{12}$ (LCO-LLZTO) on an industrial scale, a water-based tape-casting process was developed, which is scalable and environmentally friendly. Additionally, the cosintering behavior of the two materials, often leading to poor electrochemical performance, was optimized via a Li_2O-rich atmosphere. The resulting dense, free-standing, and phase-pure LCO-LLZTO mixed cathodes were assembled into full cells using a dual-layer solid polymer-ceramic separator and an In–Li anode. These cells show very high utilization rates for LCO of approximately 90% at a high areal capacity of over 3 mAh cm^{-2}, demonstrating the potential of water-based tape-casting for a scalable and sustainable manufacturing of oxide-ceramic based solid-state Li batteries.

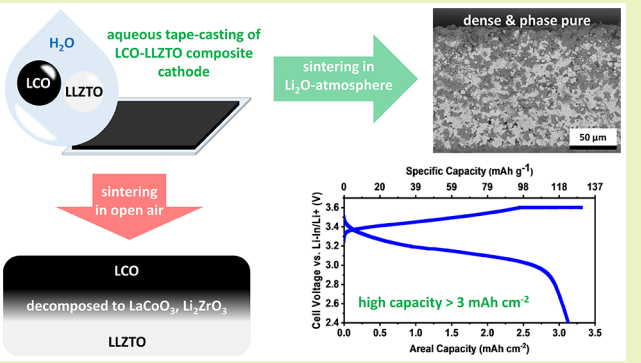

KEYWORDS: *aqueous processing, solid-state lithium batteries, composite cathode, garnet, $LiCoO_2$*

INTRODUCTION

Lithium ion batteries (LIBs) are state-of-the-art electrochemical energy storage technology, currently dominating the market for portable electronic devices and electromobility.[1] Besides the improvement of battery performance, the sustainability of LIBs production is drawing great attention, with respect to not only the raw materials but also the processing.[2−4] To that regard, aqueous processing is of great interest to reduce the environmental impact of LIBs production, e.g., reduce CO_2 emissions and carbon footprint, compared to conventional manufacturing, employing organic solvents such as hazardous *N*-methyl-2-pyrrolidione (NMP).[5] By replacing NMP or other organic solvents with water, not only is the process more environmentally benign, but also the manufacturing costs can be reduced when considering drying and solvent recovery.[6]

In the past, tremendous efforts have been made in the aqueous processing of electrodes (both cathodes and anodes) for LIBs production.[7] However, the aqueous processing of cathodes for solid-state lithium batteries (SSLBs) has been less explored. SSLBs are considered as one of the most promising next-generation secondary battery technologies, which, compared with LIBs, possess higher energy density by employing a Li metal anode and enhanced safety level by replacing the flammable organic electrolytes in LIBs with solid ones.[8,9] Previously, we developed a $LiFePO_4$ (LFP)-poly(ethylene oxide) (PEO) composite cathode for SSLBs by aqueous tape casting.[10] Due to the limit of the oxidation stability of PEO, high-voltage cathode active materials (CAMs) cannot be used in this composite cathode.[11] However, in order to obtain high energy density cathodes needed for most applications, in this work, we chose garnet-type $Li_7La_3Zr_2O_{12}$ (LLZO) and $LiCoO_2$ (LCO) to demonstrate the feasibility of aqueous processing of oxide-ceramic composite cathodes for SSLBs.

Unlike liquid or flexible polymer-based electrolytes that can effectively wet the surfaces of CAMs, the rigid garnet/CAMs interfaces need additional processing to establish good interfacial charge transfer. To obtain such interfaces, a high-temperature (>1000 °C) cosintering of these materials is usually necessary.[12] The main challenge at such a high sintering temperature is the chemical compatibility of CAMs with garnets. The decomposition reaction occurs between garnets and layer-structured cathode $LiCoO_2$ (LCO) thermodynamically above 700 °C,[13] between garnets and the spinel cathode $LiMn_2O_4$ (LMO) at 500 °C,[14] and between garnets and the olivine cathode LFP already above 400 °C.[15] Several strategies have been developed to overcome the thermal instability. By limiting the sintering temperature (1050 °C) and dwell time to 30 min, no significant decomposition was observed at the LCO/garnet interface, and good cell performance was achieved.[16] By using sintering agents such

Received: December 21, 2022
Revised: March 13, 2023
Published: March 21, 2023

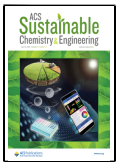

as Li_3BO_3[17,18] or $Li_{2.3}C_{0.7}B_{0.3}O_3$,[19] the cosintering temperature of LCO-garnet composite cathodes can be lowered to 700 °C. By applying advanced sintering techniques like field-assisted sintering (also referred to spark plasma sintering (FAST/SPS)), bulk highly dense LCO-garnet composite cathodes with a clear interface can be fabricated at 750 °C with a dwell time of only 10 min.[20−23] It is notable that the FAST/SPS technique is a solvent- and additive-free, energy-efficient process. However, this advanced sintering technique is facing challenges regarding upscaling.[24,25] Apart from the direct cosintering of CAMs with garnets, novel approaches are based on the infiltration of CAMs particles or their precursors into a porous garnet scaffold.[26,27] However, with such infiltration approaches, obtaining dense and thus high energy density cathodes is challenging. Thus, in the approach presented here, we explore the scalable fabrication of free-standing composite cathodes based on LCO and LLZO. We use environmentally friendly, water-based tape-casting using a biopolymer binder and subsequent cosintering. We successfully demonstrated an optimized aqueous processing and sintering route, leading to cells with high areal capacity and utilization.

EXPERIMENTAL SECTION

Preparation of LCO-LLZTO Composite Cathode. To prevent Al^{3+}/Co^{3+} interchange reaction occurring at the interface between LCO and Al-doped LLZO (Al-LLZO) during sintering,[17] the Al-free Ta-substituted $Li_{6.6}La_3Zr_{1.6}Ta_{0.4}O_{12}$ (LLZTO) is used in our work to fabricate LCO-LLZTO composite cathodes. The LLZTO powder was prepared by solid-state reaction (details in Supporting Information), and the LCO was a commercially available one (Alfa Aesar, 99.5%). For the tape-casting of the composite cathode consisting of LLZTO and LCO, a water-based slurry formulation developed for garnet separators[28] was adopted to prepare the LCO-LLZTO composite cathode. The formulation of the slurry with LLZTO and LCO powder with a weight ratio of 1:1 is summarized in Table 1. An aqueous

Table 1. Slurry Formulation for Tape-Casting of LCO-LLZTO Composite Cathode

Materials	Function	Weight Percent [%]
LLZTO	solid	26.20
LCO	solid	26.20
deionized water	solvent	43.66
methylcellulose	binder	0.44
polyethylene glycol	plasticizer	1.75
glycerol	plasticizer	1.75

polymer solution was prepared in advance by dissolving methylcellulose (Alfa Aesar), polyethylene glycol (PEG400, Merck), and glycerol (Merck, 99%) in deionized water. The LCO and LLZTO powders were added into the polymer solution. This suspension was then homogenized under vacuum (10 kPa) with 5 mm diameter ZrO_2 beads in a planetary mixer (Thinky, USA) at 1000 rpm for 5 min to form the slurry for tape-casting. Afterward, the obtained slurry was cast on a Mylar foil using a moving doctor blade. The thickness of the green tape was controlled by setting the gap of a doctor blade at 400 μm. After drying overnight at ambient atmosphere, the green tape was manually peeled off the Mylar foil.

Two layers of the composite cathode green tapes were laminated at 80 °C with an applied mechanical pressure of 250 or 500 MPa for 2 min to increase the packing density. The laminated green tapes were punched into discs with a 10 mm diameter for sintering. The prepared green tape discs were placed on an alumina plate inside an alumina crucible with or without a lid. For the case of using the closed crucible, a certain amount of LiOH powder was added around the alumina plate to create a Li_2O atmosphere when sintering. The crucibles were heated in air at a heating rate of 2 °C min^{-1} to 750 °C with 1 h dwell time and subsequently at a heating rate of 10 °C min^{-1} to 1050 °C with 6 h dwell time for sintering, followed by free cooling to room temperature. Afterward, the sintered composite cathodes were immediately transferred into an Ar-filled glovebox and stored there.

Cell Assembly. The fabrication route of the SSLB cell containing the LCO-LLZTO composite cathode is described in Figure 1. The garnet-supported LCO-based SSLB was assembled layer by layer. The freestanding garnet thin sheet fabricated by water-based tape-casting described in our previous work[28] was employed as the separator in the SSLB. After coating a thin Au layer on one side of the garnet separator, an indium foil was brought onto it to act as an anode. The purpose of using indium is to suppress lithium dendrite formation, especially for a high-capacity battery.[10] Afterward, a prepared Si-modified poly(ethylene oxide) (Si-PEO) membrane was attached onto the other side of the garnet separator, followed by placing the sintered LCO-LLZTO composited cathode on the top. Beforehand, a gold thin film was sputter-coated (20 mA, 150 s, using a desktop Cressington 108 auto coater) on the top of the sintered LCO-LLZTO composite cathode as the current collector. Due to the strong hydrogen bonding, the Si-PEO interlayer exhibited good adhesive ability so that the cathode and the separator were bonded tightly. The Si-PEO exhibits an electrochemical stability window up to 4.3 V vs Li/Li^+ (Figure S2), which is suitable for the application in the SSLB with the prepared LCO-LLZTO composite cathode. The full cells were assembled in a Swagelok-type cell. Prior to testing, the cell was stored at 80 °C overnight and cooled to 60 °C for battery testing. The theoretical areal capacity of the LCO-LLZTO composite cathode was calculated by its mass after sintering since the LCO and LLZTO have a weight ratio of 1:1 in this cathode. A typical LCO-loading in the prepared cathode was about 25.5 mg cm^{-2}, corresponding to 3.49 mAh cm^{-2} (The theoretical specific capacity of 137 mAh g^{-1}, corresponding to half of the Li removed from $LiCoO_2$).

Characterization. Inductively coupled plasma optical emission spectroscopy (ICP-OES) was used to determine the elemental stoichiometry of the LLZTO powder. X-ray diffraction (XRD) was performed on a Bruker D4 Endeavor device (Bruker, Germany) using Cu Kα radiation equipped with a LynxEye 1D detector LynxEye. Backscattering electron-scanning electron scope (BSE-SEM) images and energy-dispersive X-ray spectroscopy (EDS) analysis were taken by a Hitachi TM3000 tabletop SEM. For investigation of cross sections, samples were embedded in EpoFix epoxy resin (Struers, Germany) and mirror-polished. Prior to measurements, all samples were coated with a thin gold film to form a conductive top layer in order to avoid possible charging problems during measurements.

For testing the cycling performance of the SSLB, a formation cycle was first performed by charging to 3.6 V vs $Li-In/Li^+$ and discharging to 2.8 V vs $Li-In/Li^+$ both with a constant current density of 50 μA cm^{-2}. In the following cycles, the constant-current-constant-voltage (CC−CV) process was used for charging. The battery was charged to 3.6 V vs $Li-In/Li^+$ with a constant current density of 50 μA cm^{-2}, and was then held at the voltage until the current dropped to 5 μA cm^{-2}. Afterward, the battery was discharged to 2.4 V vs $Li-In/Li^+$ with a constant current density of 50 μA cm^{-2}.

RESULTS AND DISCUSSION

Tape Casting of LCO-LLZTO Composite Cathodes. The chemical composition of the prepared LLZTO powder was analyzed by ICP-OES, and the result (Table S1) shows that the concentration of Al is below the detection limit, indicating that Al-free LLZTO powder was successfully obtained. It is noteworthy to mention here that in this setup, the Al uptake from the crucible was also mitigated but not completely prevented. The XRD pattern in Figure S1 shows the cubic garnet phase as the main phase, while only a low intensity peak corresponding to the tetragonal garnet phase is observed. The presence of the tetragonal phase in the starting

https://doi.org/10.1021/acssuschemeng.2c07556
ACS Sustainable Chem. Eng. 2023, 11, 5184−5194

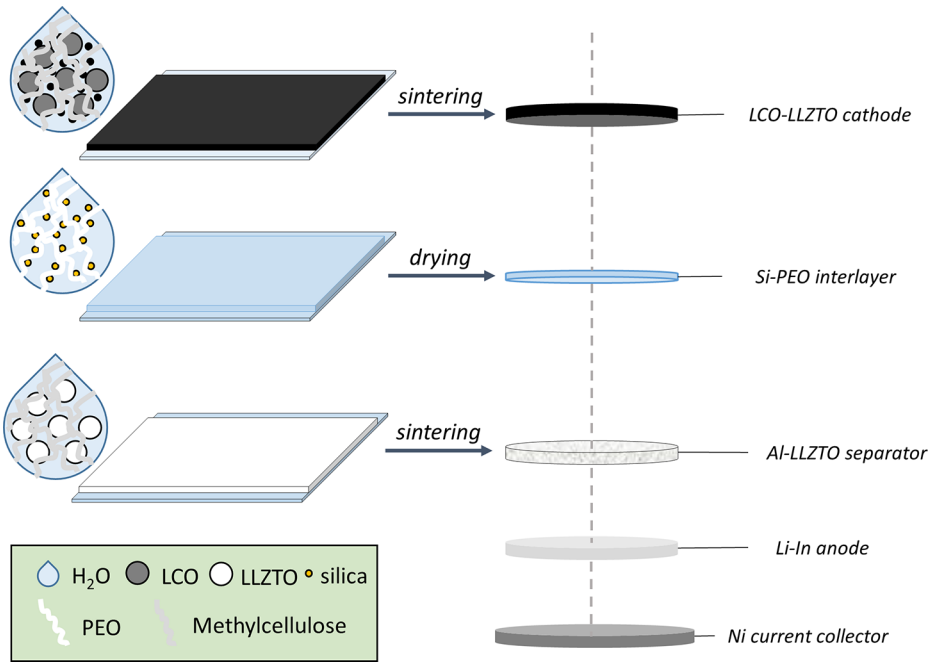

Figure 1. Schematic diagram of the water-based fabrication of the SSLB cell consisting of the LCO-LLZTO composite cathode and garnet separator.

powder is acceptable, as it will be converted to cubic phase after the aqueous processing and subsequent sintering due to the reversible Li^+/H^+ exchange (LHX).[29]

The slurry recipe for tape-casting described in our previous study[28] was taken for the tape-casting of LCO-LLZTO composite cathode tapes since the solid loading and the ratio of methylcellulose binder and the PEG-glycerol plasticizers have been optimized. For the case of the LCO-garnet composite cathode, half of the garnet powder in the original recipe was replaced by LCO and the other half by LLZTO. The high volume ratio of LLZTO in the cathode is chosen here to ensure the Li^+ percolation in the composite cathode.[16,30] The resulting green tape had a homogeneous distribution of these two solids and was flat, flexible, and easy to use for subsequent processing, e.g. shaping, and lamination (Figure 2a). As shown in Figure 2b, both the cubic garnet phase and rhombohedral LCO phase were present as the main phases in the XRD pattern of the green tape. The amount of tetragonal garnet phase was significantly reduced, because it has been partially converted to H-stabilized cubic phase due to the LHX. The exchanged Li^+ was presented in the form of Li_2CO_3 in the tape as a result of its reaction with CO_2 in air. The Li_2CO_3 serves as the Li source in the following sintering step to recover the Li content in the protonated garnet phase.

Effect of Sintering Atmosphere on Phase Purity. The cosintering step of the tape-cast mixed cathode is essential for good electrochemical performance. In practice, the LCO-LLZO mixture is considered thermally stable up to 1085 °C due to the slow kinetics of the decomposition at 700 °C.[31] However, when the aqueous LCO-LLZTO tapes were sintered in an open crucible at 1050 °C, there was a notable decomposition occurring, resulting in the formation of Li_2ZrO_3 and $LaCoO_3$, as seen in the XRD patterns (Figure 3a). When the dwell time extends to 6 h, the garnet phase was completely consumed. This indicates that the protonated LLZO has much lower thermal stability compared with the LLZO with desired stoichiometry. The possible reaction between LCO and protonated LLZO can be described as the following:

$$2Li_{7-x}H_xLa_3Zr_2O_{12} + 6LiCoO_2 \rightarrow 4Li_2ZrO_3 + 6LaCoO_3 + (3-x)Li_2O + xH_2O \quad (1)$$

The $LaCoO_3$ is a common decomposition product, which was also reported by Ren et al.[13] and Vardar et al.[32] Additionally, Vardar et al. observed $La_2Zr_2O_7$ as another main decomposition product, when annealing the LCO-LLZO half cell at 500 °C after thin-film deposition, as expressed by the reaction:[32]

$$Li_7La_3Zr_2O_{12} + LiCoO_2 \rightarrow La_2Zr_2O_7 + LaCoO_3 + 4Li_2O \quad (2)$$

However, Ren et al. did not observe the presence of $La_2Zr_2O_7$ after sintering the LCO-LLZO composite cathode at 900 °C.[13] Huang et al. suggested that $La_2Zr_2O_7$ could react with Li_2O to recover LLZO according to the following equation:[33,34]

$$3La_2Zr_2O_7 + 9Li_2O \rightarrow 2Li_7La_3Zr_2O_{12} + 2Li_2ZrO_3 \quad (3)$$

This might help explain the observed Li_2ZrO_3 phase in our experiment instead of $La_2Zr_2O_7$. The decomposition in our case might still occur according to eq 2 at lower temperatures as well, but the product $La_2Zr_2O_7$ was converted to LLZO after the reaction with Li_2O at higher temperature (~900 °C) according to eq 3. This recovery step can be accomplished fast, as there was no $La_2Zr_2O_7$ phase observed in the samples sintered, even in a quite short time (e.g., 30 min).

Other reports suggest La_2CoO_4 as a major decomposition product,[35,36] which is not the case in our sintered samples. The presence of either $LaCoO_3$ or La_2CoO_4 that are poor Li-conducting compounds will block the Li^+ transfer across the interface of LCO and LLZO, thus impeding the ionic conduction inside the composite cathode, and consequently

https://doi.org/10.1021/acssuschemeng.2c07556
ACS Sustainable Chem. Eng. 2023, 11, 5184−5194

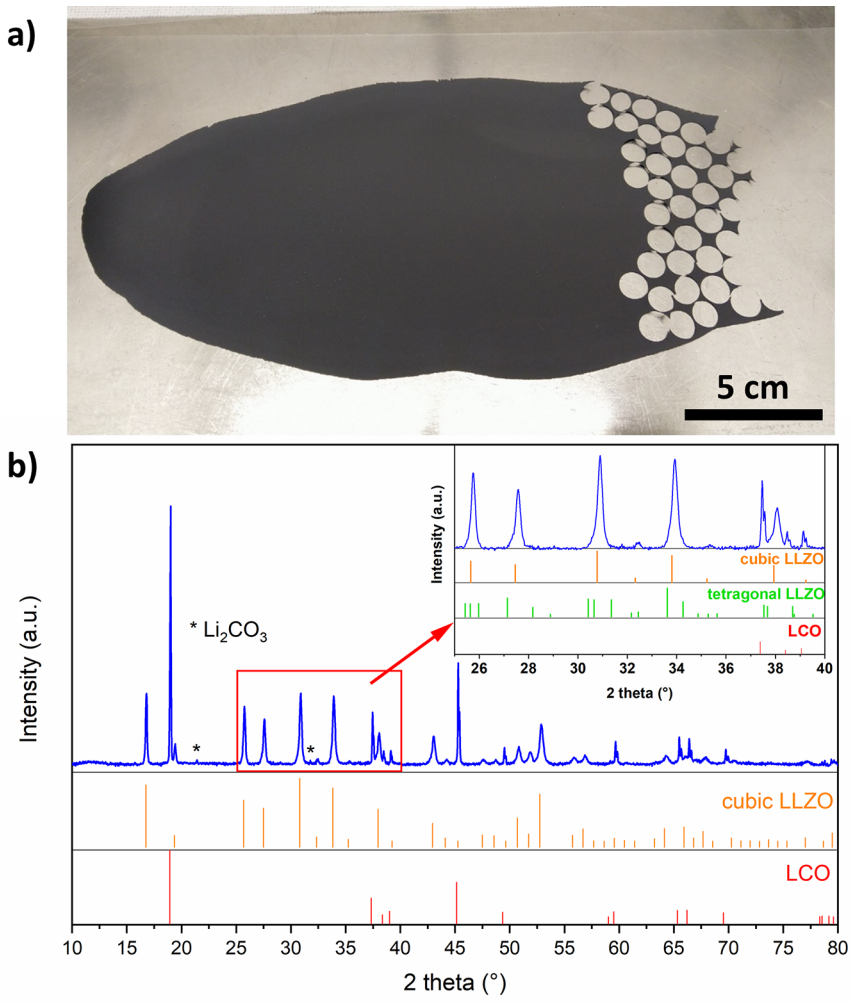

Figure 2. a) Photograph of an LCO-LLZTO composite cathode green tape fabricated by aqueous tape-casting. The tape has punched holes with a diameter of 1 cm on the right side. b) XRD pattern of the LCO-LLZTO composite cathode green tape. Reference patterns ICSD29225, ICSD182312, and ICSD246816 are used for LCO, cubic LLZO, and tetragonal LLZO, respectively.

impair the electrochemical performance of the cell. Hence, this side reaction has to be suppressed.

With a closer inspection of these equations, we can try to optimize the sintering process. The Li_2O on the right side of either eq 1 or eq 2 hints that a Li_2O atmosphere can be created in a closed crucible to suppress these decomposition reactions. Even though some parts of LLZTO decompose to $La_2Zr_2O_7$, the high Li_2O-pressure in the closed crucible can still help recover the LLZTO according to eq 3. Therefore, a certain amount of LiOH powder was intentionally added in the crucible, which releases Li_2O at 924 °C (given by the chemical supplier Alfa Aesar). As a result, there were fewer decomposition products in the samples sintered in the Li_2O-rich atmosphere (Figure 3a). LCO and LLZTO retain the main phases. Within the garnet LLZTO phase, only cubic phase is observed. This confirms the possibility to convert the tetragonal phase in the starting powder into cubic phase by the reversible LHX. The photo in Figure 3b shows the color change from black to yellowish of the sample sintered in open air, while the sample sintered in Li_2O atmosphere remains the black color, indicating no secondary phases formed due to decomposition.

Effect of Tape Compaction. The compaction of the green tape is a key step to obtain a dense cathode after sintering and thus good electrochemical performance. The green tapes were densified by means of warm pressing at 80 °C by an applied mechanical pressure of 250 and 500 MPa, respectively. The SEM images in Figure 4 show the microstructures of the fracture cross-section of the sintered LCO-LLZTO composite cathodes that were warm-pressed with 250 and 500 MPa prior to sintering. The tape pressed by 250 MPa exhibits a porous microstructure after sintering (Figure 4a-b). Although both LLZTO and LCO formed their individual percolation networks for ions and electrons, the contact between these two components were insufficient, which could lead to impaired charge transfer in this cathode or rapid fracturing during cycling. In contrast, the tapes compacted at 500 MPa are denser after sintering (Figure 4c-d), giving more contact areas between LCO and LLZTO and thus more percolation paths for Li^+ and electrons to reach the CAMs, which is important to battery performance.

Elemental Diffusion during Sintering. The composite cathode compacted at 500 MPa and subsequently sintered at 1050 °C for 6 h was analyzed by EDS for its elemental distribution. As shown in Figure 5, Al was found in the sample. The mapping of Al is overlapping with the mapping of Co, and indicates the Al^{3+}-diffusion in LCO. Since no Al was in the initial LLZTO phase, the only possible Al-source was the

https://doi.org/10.1021/acssuschemeng.2c07556
ACS Sustainable Chem. Eng. 2023, 11, 5184−5194

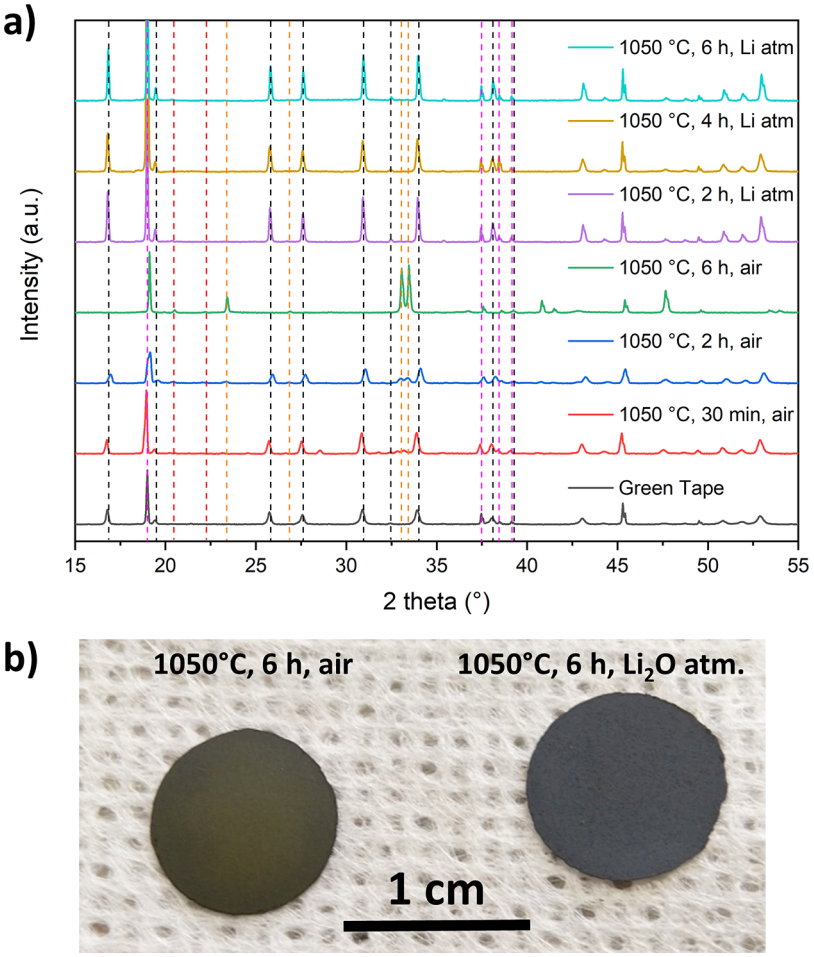

Figure 3. a) XRD patterns of LCO-LLZTO composite cathode tapes sintered at 1050 °C with various dwell times in open air or in a closed crucible filled with Li_2O-rich atmosphere (Li atm). The vertical dashed lines indicate the main reflections of cubic LLZTO (black), LCO (pink), Li_2ZrO_3 (red), and $LaCoO_3$ (orange). b) Photograph of LCO-LLZTO composite cathode tapes sintered at 1050 °C for 6 h in open air or in a closed crucible filled with Li_2O-rich atmosphere. The left one shows a yellowish color, indicating the occurrence of decomposition, while the right one maintains the black color of the green tapes.

alumina sintering substrate. The areas of the alumina substrate under the cathodes were found to be dark brownish (Figure S3), indicating the significant Al^{3+}/Co^{3+} exchange. This Al^{3+}-diffusion is not limited to the surface but through the entire cathode, which is consistent with the observation by Park et al. in the cosintered LCO and Al-doped LLZO.[17] Nevertheless, the concentration of Al is very low, as elemental analysis (Table S2) shows that the total Al-content is less than 0.02% normalized to the Co-content. In this context, the side effect of Al-contamination on the performance of LCO can be ignored. Beside the Al^{3+}-diffusion, also a minor cross-diffusion of Co into LLZO and Zr/La into LCO was observed. Such minor cross-diffusion might take place in our composite cathode as well, as dots of Co appeared in the LLZTO regions and dots of Zr/La in LCO regions. As no coherent layers were found, we estimate that the cross-diffusion of these elements is not significantly impacting the electrochemical properties. Moreover, the BSE-SEM image showed clear phase boundaries between LCO and LLZTO, and no secondary phase at the interfaces, indicating that the Co-diffusion from LCO into LLZTO and the Zr/La-diffusion from LLZTO into LCO were below the detection limit. On the other hand, spots of Al were also found in LLZTO phase but with less density. Unlike extracting Al from Al-doped LLZO that leads to low-conducting tetragonal garnet phase, the uptake of Al in the LLZTO in our composite cathode might help to stabilize the highly conductive cubic garnet phase. Therefore, an improved electrochemical performance of this LCO-LLZTO composite cathode can be expected.

Electrochemical Performance of the LCO-LLZTO Composite Cathode. The LCO-LLZTO composite cathode is prepared at a sintering temperature of 1050 °C, while the garnet separator requires a sintering temperature of 1175 °C to obtain high relative density (>90%).[28] This large difference in processing temperature hinders the fabrication of cathodic half cells in one step, i.e. laminate the cathode tapes and separator tapes together for cosintering. Therefore, these two ceramic components have to be prepared separately. When these two ceramic components are brought into contact, the rigid interface without chemical bonding raises large resistances for ionic transportation, and the cells composed of them will have low to no electrochemical performance. Therefore, the interface between the cathode and the separator needs modification. To establish a good contact at the interface, an interlayer consisting of the Li^+-conductive Si-PEO was employed. The flexibility of the polymer helps enlarge the contact area, thus providing sufficient pathways for ionic

https://doi.org/10.1021/acssuschemeng.2c07556
ACS Sustainable Chem. Eng. 2023, 11, 5184−5194

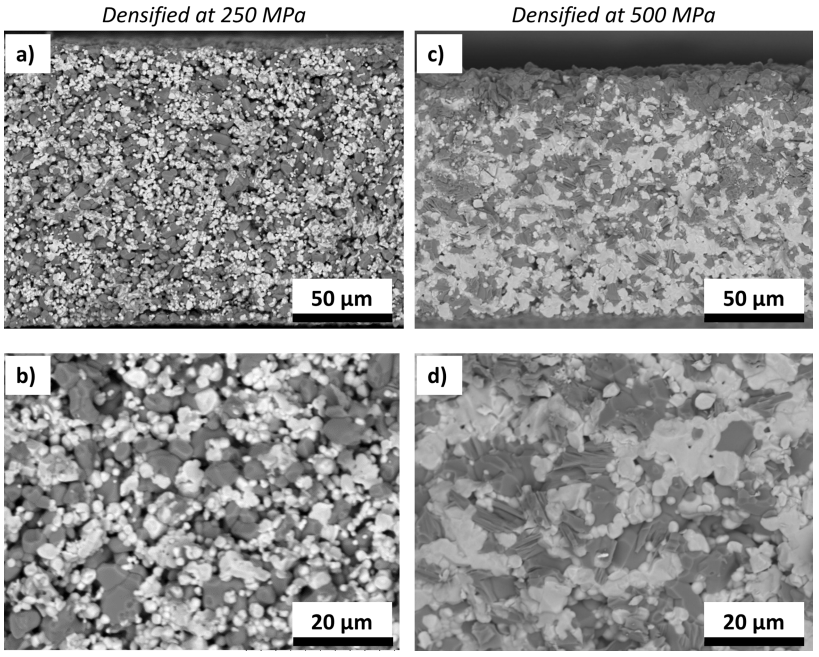

Figure 4. Cross-sectional BSE-SEM images of sintered LCO-LLZTO composite cathodes that were compacted at 80 °C with a, b) 250 MPa and c, d) 500 MPa prior to the sintering. Sintering was performed at 1050 °C for 6 h. In these images, the black, dark, and bright phases represent pores, LCO, and LLZTO, respectively.

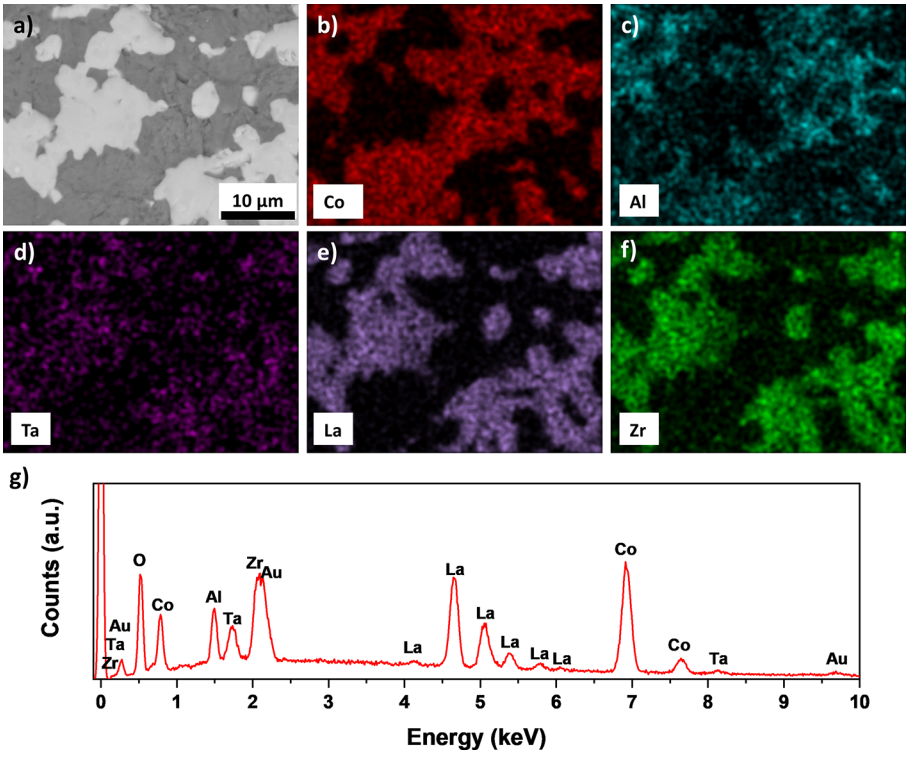

Figure 5. EDS measurement on the polished cross-section of an LCO-LLZTO composite cathode (that was compacted at 80 °C under 500 MPa and subsequently sintered at 1050 °C for 6 h). a) BSE-SEM image of the detected area. b-f) EDS mapping of the elements Co, Al, Ta, La, and Zr. g) The average spectrum of the detected area. An Au layer was sputtered onto the sample to provide sufficient electronic conductivity and explains the Au signal seen in g).

transport across the interface between the two ceramic components.[37]

The electrochemical performance of the cell was evaluated by galvanostatic cycling at 60 °C. The slightly increased temperature was required to obtain good ionic conductivity of the Si-PEO interlayer. A formation cycle was conducted with a constant current density of 50 μA cm^{-2} between 3.6 and 2.8 V vs Li−In/Li$^+$, i.e. 4.2 and 3.4 V vs Li/Li$^+$ (red curves in Figure 6a). The Coulombic efficiency of the formation cycle was 61.6%, which could be attributed to the irreversible reaction

https://doi.org/10.1021/acssuschemeng.2c07556
ACS Sustainable Chem. Eng. 2023, 11, 5184−5194

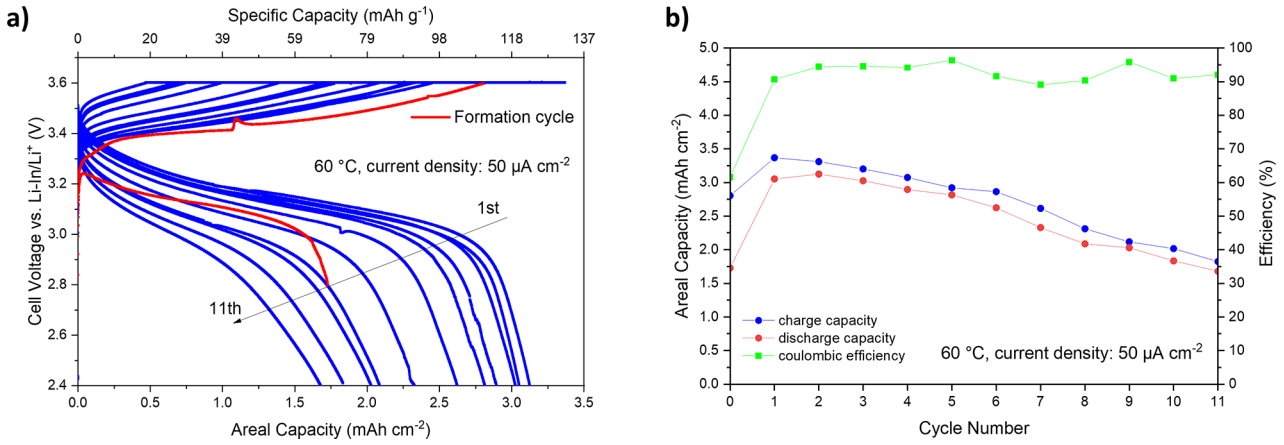

Figure 6. Electrochemical performance of the Li−In|Al-LLZTO|Si-PEO|LCO-LLZTO SSLB cell tested under the current density of 50 μA cm^{-2} at 60 °C: a) charge/discharge curves (the formation cycle is drawn in red); b) cycling performance (the formation cycle is labeled as Cycle 0).

Table 2. Overview List of LCO Cathodes for SSLBs with Garnet Separators and Their Test Conditions

Entry	Cathode Composition	LCO Loading [mg cm^{-2}]	Operation Temperature [°C]	Current Density [μA cm^{-2}]	Areal Capacity [mAh cm^{-2}]	Specific Capacity [mAh g^{-1}]	Cycles	ref
1	LCO-Li_3BO_3	2.35	25	10	0.2	85	5	38
2	LCO-Li_3BO_3-LLZO	-	r.t.	1 μA g^{-1}	-	78	1	39
3	LCO	-	50	C/5	-	35	10	17
4	LCO-Li_3BO_3	-	50	C/5	-	67.2	10	17
5	LCO-Li_3BO_3-LLZTO	-	100	100	1.40	-	50	18
6	LCO-Li_3BO_3−$In_{2(1-x)}Sn_{2x}O_3$	2.96	r.t.	5	0.056	13.9	6	40
7	LCO-Li_3BO_3−$In_{2(1-x)}Sn_{2x}O_3$	1.9	r.t.	5	0.19	101.3	5	41
8	LCO-Li_2CO_3-LLZO-$Li_{2.3}C_{0.7}B_{0.3}O_3$	1	100	5.75	0.106	106	40	19
			25	5.75	0.094	94	100	
9	LCO	-	-	2	0.015	-	3	53
10	LCO	1.52	r.t.	1	-	-	20	54
11	LCO	0.203	25	3.5	0.035	129	100	42
12	LCO with Nb coating	0.12	r.t.	1−10	0.01	80	25	36
13	LCO-LLZTO	12.6	50	50	1.6	117	100	16
14	LCO-Al-LLZTO	16	80	50	1.2	75	5	21
15	LCO-Al-LLZTO	-	80	50	0.9	-	60	22
		-	80	50	3.8	-	5	
16	LCO-Al-LLZTO	-	80	25	2.8	-	20	44
17	LCO-Al-LLZTO	2	60	25	0.27	100	6	55
18	LCO-Bi-LLZTO	4.38	60	12	0.54	124	3	56
19	LCO-Al-LLZTO	6	60	50	0.63	105	100	43
20	LCO-LLZTO	25.5	60	50	3.12	122	11	This work

involved in the Li−In alloy formation, as discussed in our previous work.[10]

The cells were further cycled with a CC−CV process for charging and a CC process for discharging between 3.6 and 2.4 V vs Li−In/Li$^+$, i.e. 4.2 and 3.0 V vs Li/Li$^+$ (blue curves in Figure 6a). The CV process allows to charge more active materials and provide a higher capacity. The cell was charged to 3.6 V vs Li−In/Li$^+$ with a constant current density of 50 μA cm^{-2}, and the voltage was held until the current density dropped to 5 μA cm^{-2}. The first charge reached a high areal capacity of 3.37 mAh cm^{-2}, indicating a high utilization of LCO up to 96%. The first discharge at 50 μA cm^{-2} delivered also high capacity over 3 mAh cm^{-2}, and the second discharge reached the highest capacity of 3.12 mAh cm^{-2}, equal to 122 mAh g^{-1} and 89% LCO-utilization. The cell showed degradation in the following cycles, and the capacity dropped to 1.68 mAh cm^{-2} at the 11th discharge (Figure 6b). The average capacity decay was 5.1% per cycle. The Coulombic efficiencies of all 11 cycles were over 90%, and most of them were around 94%. The aging mechanism behind this degradation is still not clear and thus needs further investigation.

As discussed before, a degraded LCO-LLZO interface due to the thermal-treatment-induced Al/Co cross-diffusion could be excluded in this composite cathode. This degradation mechanism proposed by Park et al. describes that the extraction of Al from LLZO leads to the disordering of cubic LLZO to tetragonal.[17] In our composite cathode, the LLZTO itself has no Al, and the Al^{3+}-diffusion into LCO solely results from the contact with the alumina substrate during sintering. Meanwhile no tetragonal LLZTO phase was detected in the sintered cathode. In addition, the SSLB with this blocking

https://doi.org/10.1021/acssuschemeng.2c07556
ACS Sustainable Chem. Eng. 2023, 11, 5184−5194

interface had a specific capacity of only 35 mAh g^{-1} (entry 3 in Table 2),[17] while the SSLB demonstrated here exhibited a much higher specific capacity (122 mAh g^{-1}). Even when Li_3BO_3 or $Li_{2.3}C_{0.7}B_{0.3}O_3$ was used as sintering additives to prevent the formation of such highly resistive interface, the maximum specific capacity reached was merely around 100 mAh g^{-1} due to the poor ionic conductivity of these additives (entries 1−8 in Table 2).[17,19,38−41] An alternative to prevent Al/Co cross-diffusion is to avoid the Al substitution in the garnet LLZTO. As a result, the thermal-induced transformation of cubic LLZO into the tetragonal phase is prevented, and highly conductive interfaces are obtained. Therefore, the use of Al-free LLZTO demonstrated in this work enables the sintering without interfacial modification, and achieves a specific capacity as high as a thin-film SSLB[42] (129 mAh g^{-1}, entry 11 in Table 2) while having more than 100-times higher LCO loading.

Possible Degradation Mechanisms. Among bulk-type cells (for instance >1 mAh cm^{-2}), the cell made by Tsai et al. via cosintering of LCO-LLZTO also exhibited similar high specific capacity of 117 mAh g^{-1} (entry 13 in Table 2).[16] A capacity decay of 2.3% per cycle based on the first 10 cycles was observed in their cells. They found the formation of microcracks due to the volume change of LCO during cycling, which they related to the degradation.[43]

Another degradation mechanism is proposed by Ihrig et al. recently, that an electrochemically driven Al/Co cross-diffusion during cycling causes the formation of an amorphous secondary phase at the interface between LCO and Al-LLZTO.[22] The as-sintered composite cathode fabricated by FAST/SPS did not show any Al/Co cross-diffusion, but Al was found in LCO after electrochemical cycling. The capacity decay per cycle in the initial 5 cycles was 8.1%, 9.4%, and 13.5% for various cathodes with areal capacities of 0.9, 1.2, and 3.8 mAh cm^{-2}, respectively (entries 14 and 15 in Table 2).[21,22] Similarly, the cathode prepared by Rosen et al. using the same materials via conventional sintering also showed an average capacity decay of 10.8% per cycle in the initial 5 cycles with the areal capacity of 3 mAh cm^{-2} (entry 16 in Table 2),[44] which could have the same degradation mechanism. In contrast, the LCO-LLZTO cathode developed in this work had an improved cycling stability with a lower capacity decay of 5.1% per cycle when the high capacity over 3 mAh cm^{-2} was achieved. Since no Al can be extracted from the LLZTO phase in our cathodes, this electrochemically driven degradation could be excluded. As there is in fact Al (diffused from alumina substrate) existing in the LCO phase of the cathode, the impact of Al on the battery performance requires further investigation. In this regard, additional experiments by sintering on different substrates can be done for a comparison to evaluate the effect of Al-doping in LCO for the LCO-garnet composite cathodes.[45]

Other degradation contributions could relate to the anode. As shown in our previous study, the Coulombic efficiency of the LFP-based SSLBs with indium anode was 96−98%, while the one of SSLBs with Li anode was 99%.[10] This means that the irreversible reaction during the Li−In alloying brings 1−3% capacity loss. Moreover, the metallic indium has poor wettability at the surface of garnets, giving rise to large resistance.[46] As shown in the Nyquist plots (Figure S4), the resistance of the garnet/anode interface has the dominant contribution to the total cell resistance.

The degradation could also relate to the decomposition of the Si-PEO interlayer. Although the voltammetry measurement shows the improved stability of this solid polymer membrane (Figure S2c), it might still form certain cathode-electrolyte interfaces due to the continuous decomposition of the polymer and the lithium salt at the high voltage (>4 V vs Li/Li^+),[47,48] which needs further investigation. The impedance of this polymer interlayer is hard to precisely distinguish from the impedance of the cathode by a simple EIS technique.[23] In this regard, advanced characterization methods and test setups are necessary to investigate the influence of the Li−In alloying process on the electrochemical performance of the garnet-based SSLBs.[49−52]

CONCLUSION

In this work, a green and environmentally friendly processing route for LCO-LLZTO composite cathodes is shown. The water-based tape-casting process developed here allows the preparation of free-standing, dense, and homogeneous LCO-LLZTO composites. The optimization of the pressing and sintering of the cathode tapes in a Li_2O-rich atmosphere reverses the water-induced LHX and stabilizes the rhombohedral LCO and cubic LLZTO phases. The resulting LCO-LLZTO interface are highly conductive and allow the cycling of the entire 100 μm-thick composite cathode in a full cell with comparably high cycling stability. In total, an areal capacity of 3.12 mAh cm^{-2}, corresponding to a specific capacity of 122 mAh g^{-1}, is achieved. These electrochemical properties are promising and demonstrate the potential of water-based tape-casting of LCO-LLZTO composites. In conclusion, oxide-based ceramic Li-ion conductors with their high total conductivity and excellent chemical and electrochemical stability enable environmentally benign and scalable fabrication routes for next-generation solid-state Li batteries.

ASSOCIATED CONTENT

Supporting Information

The Supporting Information is available free of charge at https://pubs.acs.org/doi/10.1021/acssuschemeng.2c07556.

Preparation of Al-free LLZTO powder and Si-PEO solid polymer electrolyte; ICP-OES analysis and XRD pattern of LLZTO powder; ICP-OES analysis of the composite cathode after sintering; Scheme of the synthesis mechanism, photograph, and LSV of the Si-PEO membrane; Photograph of the alumina crucible after sintering the LCO-LLZTO composite cathodes; EIS spectra of the SSLB cell and the fitting results (PDF)

AUTHOR INFORMATION

Corresponding Author

Ruijie Ye − *Institute of Energy and Climate Research − Materials Synthesis and Processing (IEK-1), Forschungszentrum Jülich GmbH, 52425 Jülich, Germany; Institute for Power Electronics and Electrical Drives (ISEA), RWTH Aachen University, 52066 Aachen, Germany;* orcid.org/0000-0002-4369-3447; Phone: +49-2461-61 96827; Email: r.ye@fz-juelich.de; Fax: +49-2461-619120

Authors

Martin Ihrig − *Institute of Energy and Climate Research − Materials Synthesis and Processing (IEK-1),*

https://doi.org/10.1021/acssuschemeng.2c07556
ACS Sustainable Chem. Eng. 2023, 11, 5184−5194

Forschungszentrum Jülich GmbH, 52425 Jülich, Germany; orcid.org/0000-0002-3616-7473

Egbert Figgemeier − *Institute for Power Electronics and Electrical Drives (ISEA), RWTH Aachen University, 52066 Aachen, Germany; Helmholtz Institute Münster (HI MS, IEK-12), Forschungszentrum Jülich GmbH, 48149 Münster, Germany*

Dina Fattakhova-Rohlfing − *Institute of Energy and Climate Research − Materials Synthesis and Processing (IEK-1), Forschungszentrum Jülich GmbH, 52425 Jülich, Germany; Faculty of Engineering and Center for Nanointegration Duisburg-Essen, University of Duisburg-Esssen, 47057 Duisburg, Germany;* orcid.org/0000-0003-2008-0151

Martin Finsterbusch − *Institute of Energy and Climate Research − Materials Synthesis and Processing (IEK-1), Forschungszentrum Jülich GmbH, 52425 Jülich, Germany; Helmholtz Institute Münster (HI MS, IEK-12), Forschungszentrum Jülich GmbH, 48149 Münster, Germany;* orcid.org/0000-0001-7027-7636

Complete contact information is available at: https://pubs.acs.org/10.1021/acssuschemeng.2c07556

Author Contributions

The manuscript was written through contributions of all authors. All authors have given approval to the final version of the manuscript.

Funding

The Ministry of Economic Affairs, Innovation, Digitalization and Energy of the State North Rhine-Westphalia in Germany, and the German Federal Ministry of Education and Research (BMBF).

Notes

The authors declare no competing financial interest.

■ ACKNOWLEDGMENTS

The Ministry of Economic Affairs, Innovation, Digitalization and Energy of the State North Rhine-Westphalia in Germany is gratefully acknowledged for funding the project "GrEEn" (project number: 313-W044B). We also gratefully acknowledge the funding by the German Federal Ministry of Education and Research (BMBF) as part of the FestBatt2-Oxide (grant no. 13XP0434A), FestBatt2-Hybride (grant no. 13XP0428A) and FestBatt-2-Prod (grant no. 13XP0432B).

■ REFERENCES

(1) Placke, T.; Kloepsch, R.; Dühnen, S.; Winter, M. Lithium ion, lithium metal, and alternative rechargeable battery technologies: the odyssey for high energy density. *J. Solid State Electrochem.* **2017**, *21* (7), 1939−1964.

(2) Armand, M.; Tarascon, J. M. Building better batteries. *Nature* **2008**, *451* (7179), 652−657.

(3) Larcher, D.; Tarascon, J. M. Towards greener and more sustainable batteries for electrical energy storage. *Nat. Chem.* **2015**, *7* (1), 19−29.

(4) Dühnen, S.; Betz, J.; Kolek, M.; Schmuch, R.; Winter, M.; Placke, T. Toward Green Battery Cells: Perspective on Materials and Technologies. *Small Methods* **2020**, *4* (7), 2000039.

(5) Bresser, D.; Buchholz, D.; Moretti, A.; Varzi, A.; Passerini, S. Alternative binders for sustainable electrochemical energy storage - the transition to aqueous electrode processing and bio-derived polymers. *Energ Environ. Sci.* **2018**, *11* (11), 3096−3127.

(6) Wood, D. L.; Li, J.; Daniel, C. Prospects for reducing the processing cost of lithium ion batteries. *J. Power Sources* **2015**, *275*, 234−242.

(7) Liu, H.; Cheng, X.; Chong, Y.; Yuan, H.; Huang, J.-Q.; Zhang, Q. Advanced electrode processing of lithium ion batteries: A review of powder technology in battery fabrication. *Particuology* **2021**, *57*, 56−71.

(8) Janek, J.; Zeier, W. G. A solid future for battery development. *Nat. Energy* **2016**, *1*, 16141.

(9) Manthiram, A.; Yu, X. W.; Wang, S. F. Lithium battery chemistries enabled by solid-state electrolytes. *Nat. Rev. Mater.* **2017**, *2* (4), 16103.

(10) Ye, R.; Hamzelui, N.; Ihrig, M.; Finsterbusch, M.; Figgemeier, E. Water-Based Fabrication of a LilLi7La3Zr2O12lLiFePO4 Solid-State Battery—Toward Green Battery Production. *ACS Sustainable Chem. Eng.* **2022**, *10* (23), 7613−7624.

(11) Homann, G.; Stolz, L.; Nair, J.; Laskovic, I. C.; Winter, M.; Kasnatscheew, J. Poly(Ethylene Oxide)-based Electrolyte for Solid-State-Lithium-Batteries with High Voltage Positive Electrodes: Evaluating the Role of Electrolyte Oxidation in Rapid Cell Failure. *Sci. Rep-Uk* **2020**, *10* (1), 4390.

(12) Tsai, C.-L.; Yu, S.; Tempel, H.; Kungl, H.; Eichel, R.-A. All-ceramic Li batteries based on garnet structured Li7La3Zr2O12. *Materials Technology* **2020**, *35* (9−10), 656−674.

(13) Ren, Y.; Liu, T.; Shen, Y.; Lin, Y.; Nan, C.-W. Chemical compatibility between garnet-like solid state electrolyte Li6.75-La3Zr1.75Ta0.25O12 and major commercial lithium battery cathode materials. *Journal of Materiomics* **2016**, *2* (3), 256−264.

(14) Miara, L.; Windmuller, A.; Tsai, C. L.; Richards, W. D.; Ma, Q. L.; Uhlenbruck, S.; Guillon, O.; Ceder, G. About the Compatibility between High Voltage Spinel Cathode Materials and Solid Oxide Electrolytes as a Function of Temperature. *Acs Appl. Mater. Inter* **2016**, *8* (40), 26842−26850.

(15) Wakasugi, J.; Munakata, H.; Kanamura, K. Thermal Stability of Various Cathode Materials against $Li_{6.25}Al_{0.25}La_3Zr_2O_{12}$ Electrolyte. *Electrochemistry* **2017**, *85* (2), 77−81.

(16) Tsai, C.-L.; Ma, Q.; Dellen, C.; Lobe, S.; Vondahlen, F.; Windmüller, A.; Grüner, D.; Zheng, H.; Uhlenbruck, S.; Finsterbusch, M.; Tietz, F.; Fattakhova-Rohlfing, D.; Buchkremer, H. P.; Guillon, O. A garnet structure-based all-solid-state Li battery without interface modification: resolving incompatibility issues on positive electrodes. *Sustain Energ Fuels* **2019**, *3* (1), 280−291.

(17) Park, K.; Yu, B.-C.; Jung, J.-W.; Li, Y.; Zhou, W.; Gao, H.; Son, S.; Goodenough, J. B. Electrochemical Nature of the Cathode Interface for a Solid-State Lithium-Ion Battery: Interface between LiCoO2 and Garnet-Li7La3Zr2O12. *Chem. Mater.* **2016**, *28* (21), 8051−8059.

(18) Zheng, C.; Tang, S.; Wen, F.; Peng, J.; Yang, W.; Lv, Z.; Wu, Y.; Tang, W.; Gong, Z.; Yang, Y. Reinforced Cathode | Garnet Interface for High-Capacity All-Solid-State Batteries. *Materials Futures* **2022**, *1* (4), 045103.

(19) Han, F.; Yue, J.; Chen, C.; Zhao, N.; Fan, X.; Ma, Z.; Gao, T.; Wang, F.; Guo, X.; Wang, C. Interphase Engineering Enabled All-Ceramic Lithium Battery. *Joule* **2018**, *2* (3), 497−508.

(20) Laptev, A. M.; Zheng, H.; Bram, M.; Finsterbusch, M.; Guillon, O. High-pressure field assisted sintering of half-cell for all-solid-state battery. *Mater. Lett.* **2019**, *247*, 155−158.

(21) Ihrig, M.; Finsterbusch, M.; Tsai, C.-L.; Laptev, A. M.; Tu, C.-h.; Bram, M.; Sohn, Y. J.; Ye, R.; Sevinc, S.; Lin, S.-k.; et al. Fattakhova-Rohlfing, D.; Guillon, O. Low temperature sintering of fully inorganic all-solid-state batteries − Impact of interfaces on full cell performance. *J. Power Sources* **2021**, *482*, 228905.

(22) Ihrig, M.; Finsterbusch, M.; Laptev, A. M.; Tu, C.-h.; Tran, N. T. T.; Lin, C.-a.; Kuo, L.-Y.; Ye, R.; Sohn, Y. J.; Kaghazchi, P.; Lin, S.-k.; Fattakhova-Rohlfing, D.; Guillon, O. Study of LiCoO2/Li7La3Zr2O12:Ta Interface Degradation in All-Solid-State Lithium Batteries. *Acs Appl. Mater. Inter* **2022**, *14* (9), 11288−11299.

(23) Ihrig, M.; Ye, R.; Laptev, A. M.; Grüner, D.; Guerdelli, R.; Scheld, W. S.; Finsterbusch, M.; Wiemhöfer, H.-D.; Fattakhova-Rohlfing, D.; Guillon, O. Polymer−Ceramic Composite Cathode with Enhanced Storage Capacity Manufactured by Field-Assisted Sintering

and Infiltration. *ACS Applied Energy Materials* **2021**, *4* (10), 10428−10432.
(24) Bram, M.; Laptev, A. M.; Mishra, T. P.; Nur, K.; Kindelmann, M.; Ihrig, M.; Pereira da Silva, J. G.; Steinert, R.; Buchkremer, H. P.; Litnovsky, A.; Klein, F.; Gonzalez-Julian, J.; Guillon, O. Application of Electric Current-Assisted Sintering Techniques for the Processing of Advanced Materials. *Adv. Eng. Mater.* **2020**, *22* (6), 2000051.
(25) Chen, C.; Wang, K.; He, H.; Hanc, E.; Kotobuki, M.; Lu, L. Processing and Properties of Garnet-Type Li7La3Zr2O12 Ceramic Electrolytes. *Small* **2022**, 2205550.
(26) Ren, Y.; Liu, T.; Shen, Y.; Lin, Y.; Nan, C.-W. Garnet-type oxide electrolyte with novel porous-dense bilayer configuration for rechargeable all-solid-state lithium batteries. *Ionics* **2017**, *23* (9), 2521−2527.
(27) Kim, K.; Rupp, J. L. M. All Ceramic Cathode Composite Design and Manufacturing towards Low Interfacial Resistance for Garnet-Based Solid-State Batteries. *Energ Environ. Sci.* **2020**, *13*, 4930−4945.
(28) Ye, R.; Tsai, C.-L.; Ihrig, M.; Sevinc, S.; Rosen, M.; Dashjav, E.; Sohn, Y. J.; Figgemeier, E.; Finsterbusch, M. Water-based fabrication of garnet-based solid electrolyte separators for solid-state lithium batteries. *Green Chem.* **2020**, *22*, 4952−4961.
(29) Ye, R.; Ihrig, M.; Imanishi, N.; Finsterbusch, M.; Figgemeier, E. A Review on Li+/H+ Exchange in Garnet Solid Electrolytes: From Instability against Humidity to Sustainable Processing in Water. *ChemSusChem* **2021**, *14* (20), 4397−4407.
(30) Finsterbusch, M.; Danner, T.; Tsai, C.-L.; Uhlenbruck, S.; Latz, A.; Guillon, O. High Capacity Garnet-Based All-Solid-State Lithium Batteries: Fabrication and 3D-Microstructure Resolved Modeling. *Acs Appl. Mater. Inter* **2018**, *10* (26), 22329−22339.
(31) Uhlenbruck, S.; Dornseiffer, J.; Lobe, S.; Dellen, C.; Tsai, C.-L.; Gotzen, B.; Sebold, D.; Finsterbusch, M.; Guillon, O. Cathode-electrolyte material interactions during manufacturing of inorganic solid-state lithium batteries. *Journal of Electroceramics* **2017**, *38* (2), 197−206.
(32) Vardar, G.; Bowman, W. J.; Lu, Q.; Wang, J.; Chater, R. J.; Aguadero, A.; Seibert, R.; Terry, J.; Hunt, A.; Waluyo, I.; Fong, D. D.; Jarry, A.; Crumlin, E. J.; Hellstrom, S. L.; Chiang, Y.-M.; Yildiz, B. Structure, Chemistry, and Charge Transfer Resistance of the Interface between Li7La3Zr2O12 Electrolyte and LiCoO2 Cathode. *Chem. Mater.* **2018**, *30* (18), 6259−6276.
(33) Huang, X.; Shen, C.; Rui, K.; Jin, J.; Wu, M.; Wu, X.; Wen, Z. Influence of La2Zr2O7 Additive on Densification and Li+ Conductivity for Ta-Doped Li7La3Zr2O12 Garnet. *JOM* **2016**, *68* (10), 2593−2600.
(34) Huang, X.; Lu, Y.; Song, Z.; Rui, K.; Wang, Q.; Xiu, T.; Badding, M. E.; Wen, Z. Manipulating Li2O atmosphere for sintering dense Li7La3Zr2O12 solid electrolyte. *Energy Storage Materials* **2019**, *22*, 207−217.
(35) Kim, K. H.; Iriyama, Y.; Yamamoto, K.; Kumazaki, S.; Asaka, T.; Tanabe, K.; Fisher, C. A. J.; Hirayama, T.; Murugan, R.; Ogumi, Z. Characterization of the interface between LiCoO2 and Li7La3Zr2O12 in an all-solid-state rechargeable lithium battery. *J. Power Sources* **2011**, *196* (2), 764−767.
(36) Kato, T.; Hamanaka, T.; Yamamoto, K.; Hirayama, T.; Sagane, F.; Motoyama, M.; Iriyama, Y. In-situ Li7La3Zr2O12/LiCoO2 interface modification for advanced all-solid-state battery. *J. Power Sources* **2014**, *260*, 292−298.
(37) Ihrig, M.; Dashjav, E.; Laptev, A. M.; Ye, R.; Grüner, D.; Ziegner, M.; Odenwald, P.; Finsterbusch, M.; Tietz, F.; Fattakhova-Rohlfing, D.; Guillon, O. Increasing the performance of all-solid-state Li batteries by infiltration of Li-ion conducting polymer into LFP-LATP composite cathode. *J. Power Sources* **2022**, *543*, 231822.
(38) Ohta, S.; Komagata, S.; Seki, J.; Saeki, T.; Morishita, S.; Asaoka, T. All-solid-state lithium ion battery using garnet-type oxide and Li3BO3 solid electrolytes fabricated by screen-printing. *J. Power Sources* **2013**, *238*, 53−56.
(39) Ohta, S.; Seki, J.; Yagi, Y.; Kihira, Y.; Tani, T.; Asaoka, T. Co-sinterable lithium garnet-type oxide electrolyte with cathode for all-solid-state lithium ion battery. *J. Power Sources* **2014**, *265*, 40−44.
(40) Liu, T.; Ren, Y.; Shen, Y.; Zhao, S.-X.; Lin, Y.; Nan, C.-W. Achieving high capacity in bulk-type solid-state lithium ion battery based on Li6.75La3Zr1.75Ta0.25O12 electrolyte: Interfacial resistance. *J. Power Sources* **2016**, *324*, 349−357.
(41) Liu, T.; Zhang, Y.; Chen, R.; Zhao, S.-X.; Lin, Y.; Nan, C.-W.; Shen, Y. Non-successive degradation in bulk-type all-solid-state lithium battery with rigid interfacial contact. *Electrochem. Commun.* **2017**, *79*, 1−4.
(42) Ohta, S.; Kobayashi, T.; Seki, J.; Asaoka, T. Electrochemical performance of an all-solid-state lithium ion battery with garnet-type oxide electrolyte. *J. Power Sources* **2012**, *202*, 332−335.
(43) Hou, A.-Y.; Huang, C.-Y.; Tsai, C.-L.; Huang, C.-W.; Schierholz, R.; Lo, H.-Y.; Tempel, H.; Kungl, H.; Eichel, R.-A.; Chang, J.-K.; Wu, W.-W. All-Solid-State Garnet-Based Lithium Batteries at Work−In Operando TEM Investigations of Delithiation/Lithiation Process and Capacity Degradation Mechanism. *Advanced Science* **2023**, *10*, 2205012.
(44) Rosen, M.; Finsterbusch, M.; Guillon, O.; Fattakhova-Rohlfing, D. Free standing dual phase cathode tapes − scalable fabrication and microstructure optimization of garnet-based ceramic cathodes. *Journal of Materials Chemistry A* **2022**, *10*, 2320−2326.
(45) Ihrig, M.; Kuo, L.-Y.; Lobe, S.; Laptev, A. M.; Lin, C.-a.; Tu, C.-h.; Ye, R.; Kaghazchi, P.; Cressa, L.; Eswara, S.; Lin, S.-k.; Guillon, O.; Fattakhova-Rohlfing, D.; Finsterbusch, M. Thermal Recovery of the Electrochemically Degraded LiCoO2/Li7La3Zr2O12:Al,Ta Interface in an All-Solid-State Lithium Battery. *Acs Appl. Mater. Inter* **2023**, *15* (3), 4101−4112.
(46) Il'ina, E. A.; Druzhinin, K. V.; Lyalin, E. D.; Plekhanov, M. S.; Talankin, I. I.; Antonov, B. D.; Pankratov, A. A. Li-In alloy: preparation, properties, wettability of solid electrolytes based on Li7La3Zr2O12. *J. Mater. Sci.* **2022**, *57*, 1291−1301.
(47) Su, S.; Ma, J.; Zhao, L.; Lin, K.; Li, Q.; Lv, S.; Kang, F.; He, Y.-B. Progress and perspective of the cathode/electrolyte interface construction in all-solid-state lithium batteries. *Carbon Energy* **2021**, *3* (6), 866−894.
(48) Li, J.; Ji, Y.; Song, H.; Chen, S.; Ding, S.; Zhang, B.; Yang, L.; Song, Y.; Pan, F. Insights Into the Interfacial Degradation of High-Voltage All-Solid-State Lithium Batteries. *Nano-Micro Letters* **2022**, *14* (1), 191.
(49) Santhosha, A. L.; Medenbach, L.; Buchheim, J. R.; Adelhelm, P. The Indium−Lithium Electrode in Solid-State Lithium-Ion Batteries: Phase Formation, Redox Potentials, and Interface Stability. *Batteries & Supercaps* **2019**, *2* (6), 524−529.
(50) Lu, Y.; Zhao, C.-Z.; Zhang, R.; Yuan, H.; Hou, L.-P.; Fu, Z.-H.; Chen, X.; Huang, J.-Q.; Zhang, Q. The carrier transition from Li atoms to Li vacancies in solid-state lithium alloy anodes. *Sci. Adv.* **2021**, *7* (38), eabi5520.
(51) Tan, D. H. S.; Banerjee, A.; Chen, Z.; Meng, Y. S. From nanoscale interface characterization to sustainable energy storage using all-solid-state batteries. *Nat. Nanotechnol.* **2020**, *15* (3), 170−180.
(52) Xiang, Y.; Li, X.; Cheng, Y.; Sun, X.; Yang, Y. Advanced characterization techniques for solid state lithium battery research. *Mater. Today* **2020**, *36*, 139−157.
(53) Kotobuki, M.; Munakata, H.; Kanamura, K.; Sato, Y.; Yoshida, T. Compatibility of Li7La3Zr2O12 Solid Electrolyte to All-Solid-State Battery Using Li Metal Anode. *J. Electrochem. Soc.* **2010**, *157* (10), A1076−A1079.
(54) Kotobuki, M.; Kanamura, K.; Sato, Y.; Yoshida, T. Fabrication of all-solid-state lithium battery with lithium metal anode using Al2O3-added Li7La3Zr2O12 solid electrolyte. *J. Power Sources* **2011**, *196* (18), 7750−7754.
(55) Scheld, W. S.; Lobe, S.; Dellen, C.; Ihrig, M.; Häuschen, G.; Hoff, L. C.; Finsterbusch, M.; Uhlenbruck, S.; Guillon, O.; Fattakhova-Rohlfing, D. Rapid thermal processing of garnet-based composite cathodes. *J. Power Sources* **2022**, *545*, 231872.

https://doi.org/10.1021/acssuschemeng.2c07556
ACS Sustainable Chem. Eng. 2023, 11, 5184−5194

(56) Watanabe, K.; Tashiro, A.; Ichinose, Y.; Takeno, S.; Suematsu, K.; Mitsuishi, K.; Shimanoe, K. Lowering the sintering temperature of $Li_7La_3Zr_2O_{12}$ electrolyte for co-fired all-solid-state batteries via partial Bi substitution and precise control of compositional deviation. *Journal of the Ceramic Society of Japan* **2022**, *130* (7), 416−423.

https://doi.org/10.1021/acssuschemeng.2c07556
ACS Sustainable Chem. Eng. 2023, 11, 5184−5194